Available online at www.sciencedirect.com
SCIENCE DIRECT
Icarus 183 (2006) 179–185
ICARUS
www.elsevier.com/locate/icarus

Discovery and characteristics of the Kuiper belt binary 2003QY90

S.D. Kern [a,*], J.L. Elliot [a,b,c]

[a] *Department of Earth, Atmospheric, and Planetary Sciences, Massachusetts Institute of Technology, Cambridge, MA 02139, USA*
[b] *Department of Physics, Massachusetts Institute of Technology, Cambridge, MA 02139, USA*
[c] *Lowell Observatory, 1400 W. Mars Hill Road, Flagstaff, AZ 86001, USA*

Received 29 December 2004; revised 27 December 2005

Available online 17 February 2006

Abstract

We present photometric and astrometric results from four epochs of ground-based observations at the Magellan telescopes of the Kuiper belt binary 2003QY90. Resolved observations show both components to be highly variable and often of nearly equal brightness, causing difficulty in distinguishing between the primary and secondary components for observations spaced widely in time. Resolved lightcurve observations on one night show one component to have a single-peaked rotation period of 3.4 ± 1.1 h and a peak-to-peak amplitude of 0.34 ± 0.12 mag. The other component exhibits a less constrained lightcurve, with a single-peaked rotation period of 7.1 ± 2.9 h and a peak-to-peak amplitude of 0.90 ± 0.36 mag. Under the assumption of equal albedos, the diameter ratio is 1.25 ± 0.11 in the Sloan i' filter. While we cannot determine an orbit from our four distinct epochs of observation (due to ambiguity in component identification), we place limits on the orbital period of the system of 300–600 days, we find a minimum semi-major axis of 13,092 km for a circular orbit and a system mass range of (2.3–18.0) $\times 10^{17}$ kg depending on the identification of components in our observations.

Keywords: Kuiper belt objects; Photometry; Satellites, general

1. Introduction

Binaries provide opportunities to measure quantities of interest in the Kuiper belt that are otherwise unobtainable without visitation. The system mass can be determined if an orbit can be established. If the body diameters can also be measured through mutual occultations and eclipses, then densities and albedos can be determined. From the densities, one can infer bulk composition and make inferences about internal structure (i.e., whether the body is a rubble pile or solid).

The mass contained within the Kuiper belt is key to our understanding of the structure and formation of the Kuiper belt as a whole (Morbidelli et al., 2003). Proposed formation models for Kuiper belt binaries (KBBs) require a massive and dynamically cold primordial disk (Goldreich et al., 2002; Weidenschilling, 2002; Funato et al., 2003; Astakhov et al., 2005). Edgeworth's (1949) original rationale for a belt of objects was based on the idea that the distribution of mass beyond the known planets should not end abruptly. Our current understanding of the belt suggests that nearly 99% of the initial mass is no longer present (Morbidelli et al., 2003). Where this mass went is still under investigation. Recent albedo measurements of KBOs (Grundy et al., 2005) suggest higher albedos than have been previously assumed, which imply lower masses than have been inferred in the past, and thus exacerbating this problem of missing mass. Characterization of KBBs helps us to establish the actual masses of objects within the belt, and their orbital and rotational characteristics may provide insight for their formation. Their existence places requirements on formation models of the belt as a whole. The more constraints we can put on the models and the more realistic values we have for input parameters, the closer we come to understanding how our Solar System formed.

Currently twenty-three KBBs (including Pluto) have been discovered, and of these, orbits have been established for about half. 2003QY90 is one of the minority without a preliminary orbit, primarily because of its relatively recent discovery at the end of 2003. Orbital periods for binaries (exclud-

* Corresponding author. Fax: +1 617 253 2886.
E-mail address: susank@mit.edu (S.D. Kern).

0019-1035/$ – see front matter
doi:10.1016/j.icarus.2006.01.002

ing Pluto, which is significantly more massive than the others) range from 19 to 825 days, with masses ranging from (0.42–13.9) $\times 10^{18}$ kg (Noll, 2003). Estimates for albedo based on a density of 1000 kg/m^3 range from very dark, 1998WW31 at 5.4% (Veillet et al., 2002), to very bright, 1997CQ29 at 37–41% (Noll et al., 2004b; Margot et al., 2004). The orbits of binaries with the exception of Pluto–Charon do not appear to be circular, with their eccentricities covering a wide range of values from 0.25 to 0.8 (Noll et al., 2004a, 2004b; Osip et al., 2003; Veillet et al., 2002; Margot et al., 2004; Kern, 2005). Proposed formation mechanisms predict a spectrum of possible configurations for binary systems: widely separated binaries (Weidenschilling, 2002), close binaries (Goldreich et al., 2002), binaries with equal mass, large separation and highly eccentric orbits (Funato et al., 2003), and perhaps the model closest to what is observed for current systems, equal mass binaries with moderately eccentric orbits and a small population of asymmetric mass KBBs (Astakhov et al., 2005). Given the properties of the close binaries currently characterized (Noll et al., 2004a, 2004b; Margot et al., 2004), one might expect 2003QY90 to have a relatively high albedo, ∼20%, a moderate eccentricity and an orbital period greater than 100 days.

2. Observations

2003QY90 was discovered by the Deep Ecliptic Survey (DES, Millis et al., 2002; Elliot et al., 2005) on 2003 August 24 at Cerro Tololo Inter-American Observatory (CTIO) using the Mosaic Camera on the Blanco 4-m telescope. It was observed two months later by the Clay 6.5-m Magellan telescope as part of the MIT recovery program for DES objects. Images under 0.5 arcsec seeing conditions recorded with the Raymond and Beverly Sackler Magellan Instant Camera (MagIC, Osip et al., 2004), a high resolution imager with 0.069 arcsec/pixel revealed 2003QY90 to be binary in nature with a separation of 0.41 ± 0.02 arcsec (updated from the value reported in the IAUC for improved image calibration, Elliot, 2003).

We have continued our observations of this object and present a log of our observations in Table 1 and sample images from each night of observation (Fig. 1) where resolved images were collected. Notice that the brightness of the components is comparable in most cases and that in panels (c) and (d), the component that appears brighter reversed between nights. We define the primary to be the component with the brighter average magnitude in lightcurve observations in 2004 September. A sample image for this time is found in panel (b) of Fig. 1.

Additional observations of the binary, in some cases resolved and in other cases unresolved, reveal that dynamically this pair resides securely in the classical population of the Kuiper belt (Elliot et al., 2005) with a heliocentric semi-major axis of 42.795 ± 0.005 AU, an eccentricity of 0.0510 ± 0.0001 and an inclination of 3.772 ± 0.001 deg. After recovery in 2004 and 2005, observations were linked back to an earlier DES detection in 2000 giving this pair a 4.78-year arc on its heliocentric orbital position.

A point-spread-function (PSF) fitting method was employed to determine the geometry of 2003QY90 during the observations. A circular Lorentzian PSF model (Bosh et al., 1992) was fit to multiple field stars in the same frame as the binary. A master PSF was constructed from those stars that produced consistent PSF parameters, where the reference star for this fit was chosen to be the brightest star of the set that was non-variable from circular aperture photometry. These stars were ∼1–4 mag brighter than the magnitude of the combined KBB system. Lastly, the binary components (separation and light ratio) were fit as separate sources in a common weighted fit with the reference stars. After the fitting was complete, the instrumental magnitude of the reference star, determined from circular-aperture photometry, and the fitted ratios for the other reference stars and KBB components were used to calculate refined instrumental magnitudes for all the fitted sources. These instrumental magnitudes were then calibrated with standard stars.

We examined the residuals from the PSF fit as a check on the model. This method works well as long as the ratio of the seeing (image FWHM) to binary separation is less than 2.0. The observations are considered in three regimes: (1) ratios <2.0, (2) ratios 2.0–3.0, and (3) ratios >3.0. Observations in regime 1 are used for binary orbit and resolved lightcurve analyses. Observations in regime 2 are primarily used for resolved lightcurve analysis and are best fit by fixing the position of the secondary relative to the primary at the position measured from resolved images on the same night or from a priori knowledge of the

Table 1
Log of observations

Observation date (UT)	No. frames	Filter	Regime	Notes
2000-Aug-27	2	VR	3	Prediscovery observations
2003-Aug-24/25	4	VR	3	Discovery of 2003QY90
2003-Sep-28	2	VR	3	Recovery observation
2003-Oct-23	3	Sloan r'	1	Binary nature discovered, binary orbit
2004-Oct-24	6	VR, Sloan r'	3	Refine astrometric position of pair
2004-May-28/29	5	Harris R	3	Refine astrometric position of pair
2004-Aug-22	5	VR	3	Refine astrometric position of pair; combined lightcurve
2004-Sep-13	6	Sloan i'	1	Lightcurve observations of individual components, binary orbit
2005-Apr-15	5	Sloan i'	3	Refine astrometric position of pair; combined lightcurve
2005-Jun-08	2	Sloan i'	1	Binary orbit
2005-Jun-09	2	Sloan i'	1	Binary orbit
2005-Jul-08	2[a]	Sloan r'	1	Binary orbit

[a] Resolved images for binary orbit, an additional 20 images in regime 2 were acquired for lightcurve observations of individual components.

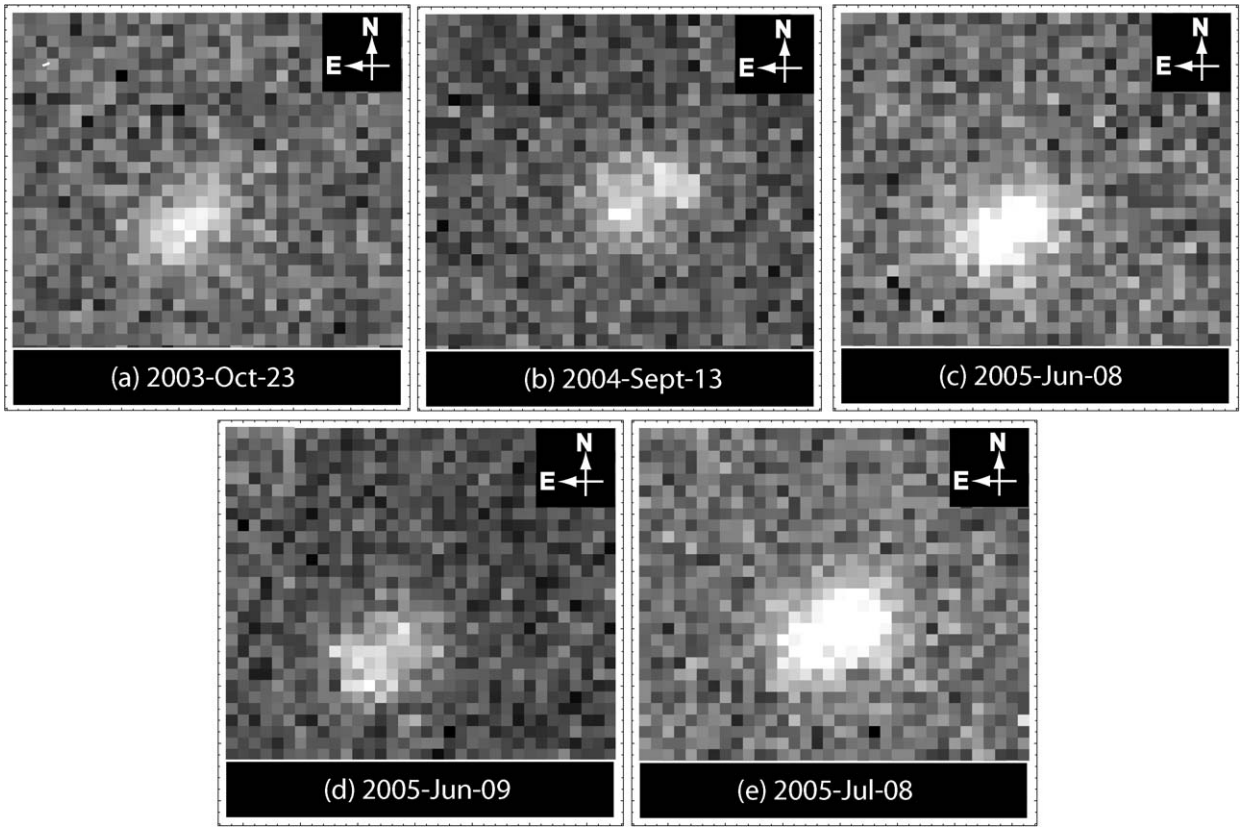

Fig. 1. Sample images taken during each epoch with MagIC (plate scale of 0.069 arcsec/pixel) on the Clay 6.5-m telescope at Las Campanas Observatory, all in better than 0.5 arcsec seeing conditions. North is up and East is to the left. Notice the comparable brightness of the components in each image.

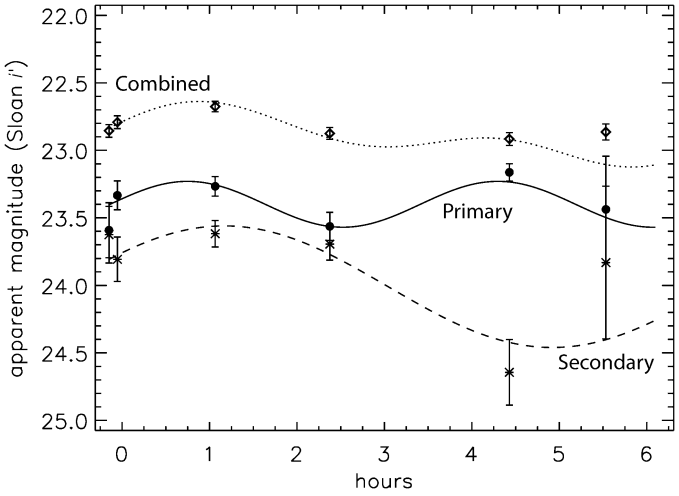

Fig. 2. Lightcurve observations for 2003QY90 collected on the night of 2004 September 13 in the Sloan i' filter. The primary lightcurve (closed circles, solid line) is fit well by a single-peaked rotation period of 3.4 ± 1.1 h with a peak-to-peak amplitude of 0.34 ± 0.12 mag and a reduced chi-square of 1.1. The secondary lightcurve (stars, dashed line) is less constrained with a reduced chi-square of 1.7, but is fit with a preliminary single-peaked rotation period of 7.1 ± 2.9 h with a peak-to-peak amplitude of 0.90 ± 0.36 mag. The third set of points (open diamonds, dotted line) is the combined light of the components overlaid with a model of the combined sinusoidal fits to the individual components. The combined light data point near 6 h has a much smaller uncertainty than the individual components since the magnitudes for the two components are negatively correlated. We include the combined lightcurve for comparison with anticipated unresolved lightcurve observations in future work. Table 2 gives additional details concerning the fits.

Table 2
Rotation period fits for 2003QY90 components on 2004 September 13

Binary component	$\bar{m}$ (mag)	$A_{\text{P-P}}$ (mag)	ϕ (°)	T (h)	Reduced χ^2
Primary	23.40 ± 0.08	0.34 ± 0.12	178 ± 34	3.4 ± 1.1	1.1
Secondary	24.01 ± 0.19	0.90 ± 0.36	206 ± 32	7.1 ± 2.9	1.7

Note. $\bar{m}$—mean magnitude of the lightcurve; $A_{\text{P-P}}$—peak-to-peak amplitude; ϕ—phase from the time of the first data point; T—single-peaked rotation period.

binary orbit if it is available. In regime 3 it is not feasible to separate the components. The described PSF fitting method was employed for all the analysis presented in this paper.

3. Lightcurves

On the night of 2004 September 13 conditions allowed for resolved photometric observations of the components of 2003QY90 for the duration of nearly 6 h. Fig. 1b is an example of the high quality data collected on this night. As a result of the excellent conditions, individual lightcurve measurements were obtained. These observations, made with the Sloan i' filter, are displayed in Fig. 2 with the best fit rotation periods overplotted. Table 2 gives the details of the resulting fits to a simple sinusoid of the form

$$m_i = \bar{m} + \frac{A_{\text{P-P}}}{2} \sin\left[\frac{2\pi(t_i - t_{\text{r}})}{T} + \phi\right], \tag{1}$$

where (m_i, t_i) are the measured magnitudes at their respective times, t_r is a reference time (the first observation of the night in the current analysis), $\bar{m}$ is the mean magnitude of the lightcurve (column 2, Table 2), $A_{P\text{-}P}$ is the peak-to-peak amplitude of the curve in magnitude (column 3, Table 2), ϕ is the phase of the curve from the time of the first data point measured in degrees (column 4, Table 2), and T is the single-peaked rotation period in hours (column 5, Table 2). Column 1 of Table 2 references the component fit and column 6 gives the reduced chi-square of the fit. The primary lightcurve is fit well by a single-peaked rotation period of 3.4 ± 1.1 h with a peak-to-peak amplitude of 0.34 ± 0.12 mag and a reduced chi-square of 1.1 (closed circles, solid line in Fig. 2). The secondary fit is less constrained with a reduced chi-square of 1.7, but yields a preliminary single-peaked rotation period of 7.1 ± 2.9 h with a peak-to-peak amplitude of 0.90 ± 0.36 (star, dashed line in Fig. 2). We have also overplotted the combined light, with the lightcurve model for the primary and secondary components (open diamonds, dotted line in Fig. 2). Since it will not always be feasible to obtain resolved lightcurve observations of this object, we wish to point out that while the combined lightcurve may be more difficult to interpret for the individual components, it still provides useful information on the system. We note that the last data point for the combined light lies significantly above the model. This is because the lightcurve model is a simple combination of the two individual models and does not take into account the magnitude correlations of the individual measurements. However, this correlation is accounted for when combining the actual magnitudes and results in smaller uncertainties on their combined light. We hope to refine our lightcurve model with observations in the future.

If these objects are triaxial ellipsoids, then the peak-to-peak amplitudes of the lightcurves for the primary and secondary components, assuming that the rotation axis of the objects are perpendicular to the line of sight, yield approximate estimates for the ratio of axis elongations of 1.4 and 2.3, respectively. The large amplitude for the secondary is close to the limit for stability from rotational fission (Leone et al., 1984); however since the uncertainty on this value is large, we do not try to interpret our result farther.

Lastly, while we have not measured accurate colors of 2003QY90, we note that the solar-phase-corrected magnitudes are ∼0.3 mag (for the primary and combined light, ∼0.15 mag for the secondary) brighter in the Sloan i' filter than the Sloan r' filter (using a phase correction coefficient of 0.14 mag/deg, Belskaya et al., 2003). Converted to the Johnson system (Smith et al., 2002), these colors fall about in the center of the current KBO color distribution for V–R (Doressoundiram, 2003).

4. Binary orbit

Astrometric measurements for the two components of 2003-QY90 have been made at four distinct epochs, however, the lightcurve effects of both components complicate our interpretation. The "primary" and "secondary" components cannot necessarily be identified by their brightness with respect to each other. Table 3 presents our observations including (1) reference epoch, (2) observation date, (3) the time span of the observations, (4) mid-time of the observations in JD, (5–6) position angle (measured from north through east) and separation in arcseconds of the identified "secondary" component, (7) the delta magnitude between components, (8–11) the filters of observation and apparent magnitude of each component and (12–14) observational parameters of geocentric distance, heliocentric distance, and phase angle.

An orbit is defined by seven orbital elements, requiring a minimum of seven measurements for a solution. Since each observation provides a pair of measurements (positions in right ascension, RA, and declination, Dec), four observations (eight measurements) are more than enough to determine an orbit. However, in the case of the 2003QY90 dataset, three epochs spaced by nearly a year each are too few for fully determining the orbit because of the ambiguity in component identification and position of the data points. For the 2004 September observations, where lightcurve information was obtained, we define the primary component to be the component that is on average brighter over our 6 h of observation. The identification of components in the discovery data are less certain as we have only three data points in time, the brightness of the components is comparable and do not vary greatly during the observations. During the 2005 June epoch, the brighter component changed between our two nights of observation. In July we have only two observations where the components are clearly resolved (as presented Table 3), however, we also continued our lightcurve

Table 3
Measured and geometric quantities

Epoch	Observation date	Δt[a] (h)	Mid-time observation (JD)	Pos. angle (°)	s_P (arcsec)	Δm (mag)	Sloan filter	Apparent magnitude			Δ[b] (AU)	r[b] (AU)	α[b] (°)
								m_{kboP}[c]	m_{kboS}[c]	m_{kboC}[c]			
2003	2003-Oct-23	1.1	2452935.53841	125 ± 5	0.41 ± 0.02	0.20 ± 0.20	r'	23.78 ± 0.10	24.03 ± 0.12	23.14 ± 0.04	44.57	44.97	1.16
2004	2004-Sep-13	5.4	2453261.61952	300 ± 3	0.38 ± 0.01	0.43 ± 0.10	i'	23.39 ± 0.17[d]	23.88 ± 0.39[d]	22.83 ± 0.09[d]	44.06	44.97	0.55
2005a	2005-Jun-08	0.8	2453529.89323	124 ± 2	0.28 ± 0.01	0.16 ± 0.10	i'	23.23 ± 0.07	23.09 ± 0.06	22.46 ± 0.03	44.62	44.97	1.22
2005a	2005-Jun-09	0.1	2453530.83826	125 ± 4	0.29 ± 0.02	-0.60 ± 0.20	i'	22.83 ± 0.10	23.40 ± 0.13	22.32 ± 0.03	44.60	44.97	1.21
2005b	2005-Jul-08	0.1	2453560.83068	118 ± 3	0.36 ± 0.01	0.16 ± 0.11	r'	23.87 ± 0.12	24.08 ± 0.16	23.22 ± 0.06	44.21	44.97	0.86

[a] Time span of observations.

[b] Δ—geocentric distance; r—heliocentric distance; α—phase angle.

[c] m_{kbpP}—apparent magnitude of the identified "primary" component; m_{kbpS}—apparent magnitude of the identified "secondary" component; m_{kboC}—apparent magnitude of the combined light of the binary components.

[d] Average magnitude; uncertainty is based on the scatter in these measurements which is greater than the formal uncertainties on the individual magnitudes due to lightcurve effects.

Table 4
Astrometry results for each resolved observation

Observation date (UT)	JD[a]	ΔRA (arcsec)	ΔDec (arcsec)	Δm (mag)	Seeing (arcsec)
2003-Oct-23	2452935.51159	0.37 ± 0.04	-0.19 ± 0.04	0.08 ± 0.26	0.49
	2452935.53841	0.21 ± 0.13	-0.17 ± 0.14	-0.40 ± 1.54	0.39
	2452935.58960	0.28 ± 0.04	-0.30 ± 0.04	0.41 ± 0.31	0.52
Average	2452935.55059	0.33 ± 0.03	-0.24 ± 0.03	0.20 ± 0.20	0.47
2004-Sep-13	2453261.54527	-0.26 ± 0.03	0.20 ± 0.04	0.03 ± 0.40	0.50
	2453261.54905	-0.36 ± 0.04	0.21 ± 0.04	0.47 ± 0.25	0.52
	2453261.59351	-0.35 ± 0.02	0.15 ± 0.02	0.35 ± 0.15	0.42
	2453261.64553	-0.33 ± 0.02	0.17 ± 0.03	0.13 ± 0.20	0.44
	2453261.72701	-0.27 ± 0.06	0.38 ± 0.06	1.48 ± 0.28	0.51
	2453261.77082	-0.29 ± 0.07	0.17 ± 0.08	0.39 ± 0.95	0.65
Average	2453261.43249	-0.32 ± 0.02	0.19 ± 0.02	0.43 ± 0.10	0.51
2005-Jun-08	2453529.87634	0.23 ± 0.01	-0.16 ± 0.02	0.26 ± 0.14	0.30
	2453529.91012	0.23 ± 0.01	-0.15 ± 0.02	0.01 ± 0.16	0.34
Average	2453529.89323	0.23 ± 0.01	-0.15 ± 0.01	0.16 ± 0.10	0.32
2005-Jun-09	2453530.83638	0.22 ± 0.03	-0.14 ± 0.03	-0.53 ± 0.35	0.39
	2453530.84014	0.26 ± 0.03	-0.19 ± 0.03	-0.64 ± 0.25	0.42
Average	2453530.83826	0.24 ± 0.02	-0.17 ± 0.02	-0.60 ± 0.20	0.41
2005-Jul-08	2453560.82880	0.33 ± 0.05	-0.16 ± 0.05	0.26 ± 0.40	0.42
	2453560.83256	0.31 ± 0.01	-0.17 ± 0.02	0.16 ± 0.12	0.40
Average	2453560.83068	0.32 ± 0.01	-0.17 ± 0.02	0.16 ± 0.11	0.41

[a] Mid-time of observations.

measurements at this time over a span of 6 h (to be presented in a future publication). Most of the images fall in regime 2. From the lightcurve we can again identify which component is on average brighter and assume that to be the primary for both the 2005 epochs. However, there is still some ambiguity since the photometric uncertainties on the 2005 dataset are large.

In Table 4 we present the position measurements for our individual observations including the (1) observation date, (2) mid-time of the observations in JD, (3–4) delta RA and Dec of the defined secondary, (5) the delta magnitude of the components (secondary to primary), and (6) the seeing in each image. Below each set of individual observations we record the weighted average position for the night.

Given our interpretation of the data points, we have attempted to search a range of possible orbits, presenting the circular orbit as a benchmark. In Fig. 3 we plot the positions of our points in each of the possible configurations. We note that the positions we observe are all close to alignment with the binary orbital plane of 2003QY90, and thus the orbit of the companion appears nearly edge-on; this alignment suggests that mutual events may be observed in the near future, or that they recently occurred.

From the times and positions, a number of constraints exist. Our observations taken in the 2005a and 2005b epochs were recorded 30.9 days apart. Since these observations were acquired close in time, we can be sure that our component identification is consistent, regardless of the brightness of the components. The secondary moves negligibly in one day and ∼6.5 deg in position angle between our observations in June and July; a rate of 0.215 deg/day. It is clear that if the orbit is circular it is significantly tilted to our line of sight. An edge-on circular orbit would appear to change little in position angle with time, while a face-on circular orbit would change relatively quickly in position angle but not in separation. Our observations indicate a change in both position angle and separation. Alternatively, the orbit could be highly elliptical.

If we interpret all our observations to be on the same side of the primary (Fig. 3, solution 1) then the period is on the order of 300 days. If the 2004 and 2005 observations are opposite each other, then the period is on the order of 600 days. For a circular orbit, we assume a minimum semi-major axis of 13,092 km (the projected separation for our farthest point). For a highly elliptical orbit, the semi-major axis is half that of the circular orbit, 6546 km. The motion of the secondary component is north through east (increasing position angle).

Based on our initial constraints for the orbital period, P, and semi-major axis, a, we calculate the system mass, m_{system}, of 2003QY90 to be in the range of (2.3–18.0) $\times 10^{17}$ kg employing the relation

$$m_{\text{system}} = 4\pi^2 a^3 / G P^2, \tag{2}$$

where G is the gravitational constant. Due to the wide range of possible periods and semi-major axes, the system mass is poorly constrained. Longer periods yield lower system masses while shorter periods yield masses more consistent with the values known for other KBB systems (Margot et al., 2004; Noll, 2003; Noll et al., 2004a, 2004b; Osip et al., 2003; Veillet et al., 2002).

Without knowledge of the actual diameter of the bodies, we cannot uniquely determine the independent values of the mean system density ρ, or the mean geometric albedo p. However, with the knowledge we do possess, we can determine a function

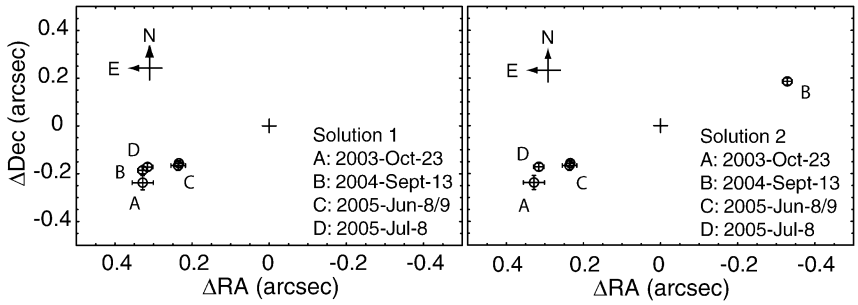

Fig. 3. Plot of the 2003QY90 positions with varied component identification for the discovery data. The data points are: (A) 2003-Oct-23, (B) 2004-Sep-13, (C) 2005-Jun-8/9, and (D) 2005-Jul-8. North is up and East is to the left. A cross denotes the position of the primary at (0, 0). Solution 1 assumes all the orbital observations are on the same side of the primary. Solution 2 assumes component identification for data in 2004 and 2005, utilizing resolved lightcurve measurements, places the secondary at opposite sides of the primary; resolved lightcurves were not acquired during the discovery epoch.

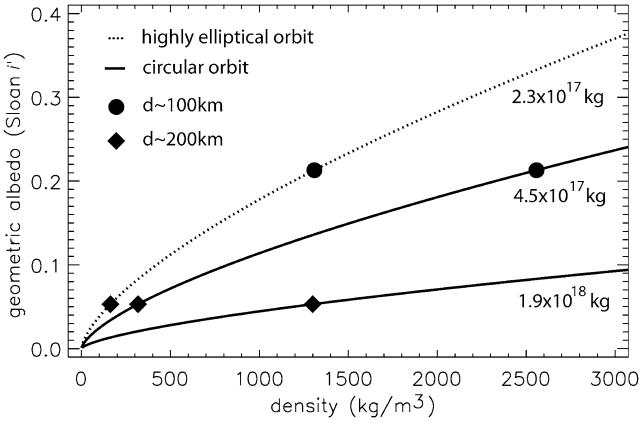

Fig. 4. Plot of geometric albedo as a function of density for a range of system masses suggested by fixing a minimum semi-major axis of 13,092 km and 6546 km for circular (solid lines) and elliptical (dotted line) orbits, respectively, and periods of 300–600 days from the position and timing information in our observations. The mass range is (2.3–18.0) $\times 10^{17}$ kg. Circles and diamonds mark the locations on each curve for assumed primary diameters of ∼100 and ∼200 km, respectively.

of these quantities, $\rho/p^{3/2}$. We define r and Δ as the heliocentric and geocentric distances to the KBO, respectively, R as the distance between the Sun and the Earth, α as the phase angle, β (0.14 mag/deg, Belskaya et al., 2003) as the phase coefficient, m_{sun} as the apparent magnitude of the Sun in the observed filter, and m_{kboP} and m_{kboS} as the apparent magnitudes of the primary and secondary components, respectively. Values for the function $\rho/p^{3/2}$ are related to our photometry and to the estimated orbital quantities (through the system mass in Eq. (2)):

$$\frac{\rho}{p^{3/2}} = \frac{3m_{\text{system}}}{4\pi}\left(\frac{R}{r\Delta}\right)^3 \left(10^{-0.6(m_{\text{sun}}-m_{\text{kboP}}-\alpha\beta)} + 10^{-0.6(m_{\text{sun}}-m_{\text{kboS}}-\alpha\beta)}\right). \quad (3)$$

Employing the transformation equations of Fukugita et al. (1996) and photometric values for the Sun in the standard Johnson–Cousins system (Cox, 2000) we find that the Sun has an apparent Sloan i' magnitude of -27.06 and apparent Sloan r' magnitude of -26.96 at the standard distance of 1.00 AU.

We use the calibrated magnitudes from the night of September 13, 2004 and plot the results for system masses corresponding to each of our orbit assumptions in Fig. 4. The solid lines mark the range of results for a circular orbit, while the dashed line marks the results for a highly elliptical orbit. Diameters (which have not yet been reported) are required to precisely determine where on this diagram the actual density and albedo of the bodies lie. For assumed diameters for the primary component of ∼100 and ∼200 km, circles and diamonds, respectively, specify the density and albedo in Fig. 4. Following our equal albedo assumption, the diameter ratio of the components is 1.25 ± 0.11 (as determined from their magnitude difference in the Sloan i' filter).

5. Conclusions

While this analysis does not uniquely describe the orbit of the binary KBO 2003QY90, it does place initial constraints on the system. We find that both components are highly variable and identification by brightness remains ambiguous until the binary orbit period can be established. Employing the positions and timing of our four epochs we infer that the orbital period is between 300 to 600 days and the minimum semi-major axis is 13,092 km for a circular orbit, 6546 km for a highly elliptical orbit. The corresponding system masses range from (2.3–18.0) $\times 10^{17}$ kg. Shorter periods correspond to the higher masses and lower albedos. If we assume equal albedos for the two components, the diameter ratio for these objects is 1.25 ± 0.11. Additionally, our measurements suggest that the orbit of the companion of 2003QY90 is close to being edge-on, making this system a possible candidate for mutual events in the near future (or recent past). Resolved lightcurve observations indicate both components to be periodic, on the order of 3.4 ± 1.1 h for one component and 7.1 ± 2.9 h for the other. While not known to great accuracy, these rotation periods are comparable to the rotation period of the secondary of 2001QT297 and of other non-binary KBOs (Sheppard and Jewitt, 2003; Osip et al., 2003). They also indicate that the objects are not in tidal lock, unlike the Pluto–Charon system, but similar to all other known KBBs.

Additional high-resolution images will be acquired of this object in the future with a combination of ground- and space-based observations. Using the current analysis as a benchmark, for a circular orbital period of ∼300 (600) days, five observations evenly spaced ∼50 (120) days apart would provide an orbit solution. If the orbit has substantial eccentricity, which

is likely given other binary orbits, then equal spacing is not optimal. However, these observations will break the ambiguity as to the identity of the components and produce an improved orbit. Further, to uniquely specify the density and albedo requires measurement of the component diameters—either with combined thermal (e.g., Spitzer) and visible observations, mutual events, or a stellar occultation.

Acknowledgments

We thank P. Schechter, R. Simcoe, J. Kane, E. Adams, and A. Vaz for their help observing at Las Campanas. We thank the telescope operators, H. Rivera, V. Meriño, G. Martin, M. Navarrete, F. Sanchez, and H. Nuñez. We also thank B. Merline for his very helpful review comments. Partial support for this work comes from NASA's Planetary Astronomy Program (Grants NAG5-10444 and NNG04GF25G) and NSF's Division for Astronomical Sciences (Grant AST-0406493).

References

Astakhov, S.A., Lee, E.A., Farrelly, D., 2005. Formation of Kuiper-belt binaries through multiple chaotic scattering encounters with low-mass intruders. Mon. Not. R. Astron. Soc. 360, 401–415.

Belskaya, I.N., Barucci, M.A., Shkuratov, Y.G., 2003. Opposition effect of Kuiper belt objects: Preliminary estimations. Earth Moon Planets 92, 201–206.

Bosh, A.S., Young, L.A., Elliot, J.L., Hammel, H.B., Baron, R.L., 1992. Photometric variability of Charon at 2.2 μm. Icarus 95, 319–324.

Cox, A., 2000. Allen's Astrophysical Quantities, fourth ed. Springer-Verlag, New York.

Doressoundiram, A., 2003. Color properties and trends in trans-neptunian objects. Earth Moon Planets 92, 131–144.

Edgeworth, K.E., 1949. The origin and evolution of the Solar System. Mon. Not. R. Astron. Soc. 109, 600–609.

Elliot, J.L., 2003. 2003QY90. IAU Circ. 8235.

Elliot, J.L., Kern, S.D., Clancy, K.B., Gulbis, A.A.S., Millis, R.L., Buie, M.W., Wasserman, L.H., Chiang, E.I., Jordan, A.B., Trilling, D.E., Meech, K.J., 2005. The Deep Ecliptic Survey: A search for Kuiper belt objects and centaurs. II. Dynamical classification, the Kuiper belt plane, and the core population. Astron. J. 129, 1117–1162.

Fukugita, M., Ichikawa, T., Gunn, J.E., Doi, M., Shimasaku, K., Schneider, D.P., 1996. The Sloan digital sky survey photometric system. Astron. J. 111, 1748–1756.

Funato, Y., Makino, J., Hut, P., Kokubo, E., Kinoshita, D., 2003. Kuiper-belt binary formation through exchange reactions. Nature 427, 518–520.

Goldreich, P., Lithwick, Y., Sari, R., 2002. Formation of Kuiper-belt binaries by dynamical friction and three-body encounters. Nature 420, 643–646.

Grundy, W., Noll, K., Stephens, D., 2005. Diverse albedos of small trans-neptunian objects. Icarus 176, 184–191.

Kern, S.D., 2005. A study of binary Kuiper belt objects. Ph.D. thesis, Earth, Atmospheric and Planetary Sciences, MIT, Cambridge.

Leone, G., Farinella, P., Paolicchi, P., Zappala, V., 1984. Equilibrium models of binary asteroids. Astron. Astrophys. 140, 265–272.

Margot, J.-L., Brown, M.E., Trujillo, C.A., Sari, R., 2004. HST observations of Kuiper belt binaries. Bull. Am. Astron. Soc. 36, 1081.

Millis, R.L., Buie, M.W., Wasserman, L.H., Elliot, J.L., Kern, S.D., Wagner, R.M., 2002. The Deep Ecliptic Survey: A search for Kuiper belt objects and centaurs. I. Description of methods and initial results. Astron. J. 123, 2083–2109.

Morbidelli, A., Brown, M.E., Levison, H.F., 2003. The Kuiper belt and its primordial sculpting. Earth Moon Planets 92, 1–27.

Noll, K., 2003. Transneptunian binaries. Earth Moon Planets 92, 395–407.

Noll, K., Stephens, D., Grundy, W., Griffin, I., 2004a. The orbit, mass, and albedo of transneptunian binary (66652) 1999RZ253. Icarus 172, 402–407.

Noll, K., Stephens, D., Grundy, W., Osip, D.J., Griffin, I., 2004b. The orbit and albedo of transneptunian binary (54534) 1997CQ29. Astron. J. 128, 2547–2552.

Osip, D.J., Kern, S.D., Elliot, J.L., 2003. Physical characterization of the binary Edgeworth–Kuiper belt object 2001QT297. Earth Moon Planets 92, 409–421.

Osip, D.J., Phillips, D.M., Bernstein, R., Burley, G., Dressler, A., Elliot, J.L., Persson, E., Shectman, S.A., Thompson, I., 2004. First-generation instruments for the Magellan telescopes: Characteristics, operation, and performance. In: Moorwood, A.F.M., Masanori, I. (Eds.), Ground-Based Instrumentation for Astronomy. SPIE, Bellingham, WA, pp. 49–59.

Sheppard, S.S., Jewitt, D., 2003. Hawaii Kuiper belt variability project: An update. Earth Moon Planets 92, 207–219.

Smith, J.A., Tucker, D.L., Kent, S., Richmond, M.W., Fukugita, M., Ichikawa, T., Ichikawa, S., Jorgensen, A.M., Uomoto, A., Gunn, J.E., Hamabe, M., Watanabe, M., Tolea, A., Henden, A.A., Annis, J., Pier, J.R., McKay, T.A., Brinkmann, J., Chen, B., Holtzman, J., Shimasaku, K., York, D.G., 2002. The $u'g'r'i'z'$ standard-star system. Astron. J. 123, 2121–2144.

Veillet, C., Parker, J.P., Griffin, I., Marsden, B., Doressoundiram, A., Buie, W.M., Tholen, D.J., Connelley, M., Holman, M.J., 2002. The binary Kuiper-belt object 1998WW31. Nature 416, 711–713.

Weidenschilling, S.J., 2002. On the origin of binary transneptunian objects. Icarus 160, 212–215.